AN ASSESSMENT OF ACOUSTIC EMISSION TECHNIQUES ON MEDIUM-SIZE PRESSURE VESSELS TESTED TO FAILURE

A.C.E. SINCLAIR, C.L. FORMBY and D.C. CONNORS

United Kingdom Atomic Authority

Risley Engineering and Materials Laboratory, Risley, Warrington WA3 6AT, United Kingdom,

SUMMARY

Location analysis has been used to examine acoustic emission from a partial thickness slit in a test vessel during pressurization. Preliminary investigations showed that sharp emission pulses at a source would propagate as sharp pulses to a sensor several metres distant, and that intrinsic material attenuation was negligible at the 165 kHz operating frequency. Pulse arrival times at three sensors were used to locate emission sources and the requirement for near-coincidence in arrival times at all sensors reduced background noise to very low levels. The slit was clearly delineated by its emissions. Emission activity moved from the centre to the ends of the slit as the stress on the slit increased, suggesting that emissions were generated during the initial yielding of the steel. This indication was strengthened by the fact that the emission count appeared to be directly proportional to the volume of plastically yielded material associated with the defect, based on a simple model for the increase in plastic zone size with pressure. Application of acoustic emission techniques to structural validation is discussed in terms of the measured amplitude spectrum of the detected acoustic emissions. A relationship is derived between the detected emission count, the threshold amplitude for detection, the sensor spacing and the created plastic volume for the steel studied.

1. INTRODUCTION

When steel is stressed it may emit acoustic energy in the form of emission pulses which propagate through the material. It is possible that detection of the emission bursts will serve to locate flaws in a structure and ultimately to offer a method for remote assessment of defect severity. Before these useful goals can be achieved considerable work is needed to determine the character and amplitude of the emissions. The dependence of the emissions on material parameters, stress conditions, thermal history, corrosion effects and in nuclear environments, the irradiation history, needs to be determined.

One important problem associated with acoustic emission detection is the often low level of signals compared with background noise, which may be electrical noise associated with the detectors and acoustic noise in the structure under test. The method of stressing the steel to produce the emissions may be inherently noisy, and background conditions in industrial structures are rarely quite. Thus we have adopted a method of multiple sensor correlation which enhances the signal-to-noise ratio. Similar systems are in use elsewhere, for example as described by Bentley et al., 1972; Parry and Robinson 1970 and Vetrano, Jolly and Hutton, 1972. Using location techniques much of the background noise can be eliminated and attenion can be focussed on the area where emissions from the material are generated. The system may be used for wide-area surveillance of structures in order to detect growing defects.

In the present report we are concerned with emissions from a defect in steel plate as the defect is stressed for the first time. This condition would be encountered during the proof test of pressure vessels. Experiments on laboratory specimens (e.g. Palmer, 1972; Nakamura et al., 1971; Bentley et al., 1973) under similar conditions have given information on the expected emission behaviour for a range of steels, and suggested that defect location would be possible. It was important to evalutate this capability on a test vessel intermediate between laboratory specimens

and full size vessels, and in a situation where defect behaviour was well understood.

2. EXPERIMENTAL DETAILS

Four acoustic sensors were mounted near a pre-machined slit in a vessel. These fed equipment for signal discrimination, time interval analysis and event location. Figure 1 shows the arrangement of equipment for the experiment. The course of pressurisation was monitored during the experiment by recording the pressure, the crack opening at the slit and the event rate from one channel. Event location proceeded in real time, using one triplet of sensors, while all four sensor signals were recorded on magnetic tape for subsequent analysis.

The cylindrical steel vessel, whose composition and treatment is listed in Table 1, was 1.52 m in diameter, 3.65 m in length, with 26.9 mm wall thickness. The internal surface of the vessel, in the area where the slit was to be machined, was polished to remove rust and greased before the vessel was filled with water. The external surface had been rust-proofed. There was thus no possibility that subsequent emissions resulted from flaking rust.

Before machining the slit, the vessel was pressurised to 1000 p.s.i. It is well known that the second stressing of a structure proceeds with far fewer acoustic events than the first. Thus acoustic activity from vessel supports, welds and seals was minimised during subsequent pressurisation of the slit.

The slit was machined on the external surface of the vessel, parallel with the vessel axis. Its depth was 16.5 mm over 370 mm length, while at each end of the slit the profile was a segmment of a circle, to give 460 mm overall length. The slit's root radius was approximately 0.1 mm. Finally the slit was packed with grease to prevent rusting and a calibrated clip gauge for measurement of the slit opening was mounted at its centre. Use of a partially penetrating rather than a through slit eliminated the need for a sealing patch which might have

generated further emissions due to sliding.

The sensors used lead zirconate titanate (PZT5A) piezoelectric material, and were constructed as shown in the insert of Figure 1, with polarisation direction normal to the mounting surface. They had maximum sensitivity at 165 kHz, with 30 kHz bandwidth, and their sensitivity was somewhat better than commercial sensors. The sensors were magnetically clamped to the vessel, using grease for acoustic coupling, to form a square array centred on the slit with 1.02 m detector spacing.

Signals were processed by specially constructed discrimination circuits so that both the height and length of the received acoustic emission pulses were used to discriminate against noise. It was found that the detectable pulse rate in the presence of noise could be almost tripled during the experiment by discriminating against pulses less than 25 μs long, as well as triggering above a preset threshold level. The discriminators also tested for the prior absence of acoustic activity before accepting emission signals over an interval which we set at 2.5 ms. This eliminated the multiplicity of outputs from a single event which otherwise could be produced by the multiply-peaked response of a sensor to the event as discussed in Section 3.

The outputs from the discriminators fed the time interval computer for event location. The method of source location and the operation of the computer have been described elsewhere (Connors, 1973; Tobias, 1973). We simply note here that for a source at location P we used a triplet of sensors, which we label M, X and Y, to produce two pairs of time differences for a given event, namely:

$$\Delta t_x = (PX - PM)/v$$

$$\Delta t_y = (PY - PM)/v$$

where v is the acoustic velocity. The time differences define two hyperbolae at whose intersection the source is located. With the geometry of the present experiment we could neglect ambiguities arising

from the multiple intersections of the hyperbolae. The time resolution of the system was 12.5 μs. The spatial resolution near the slit was approximately 25 mm.

3. PROPAGATION OF ACOUSTIC ENERGY IN VESSEL PLATE

The vessel can be adequately represented as a flat isotropic plate for our purposes. Guided acoustic waves in plates have been completely analysed - see for example Auld, 1973. One family of such waves comprise the SH (shear horizontal) waves, where the particle motion is in the plate plane. Lamb waves form another family of propagation modes, whose particle vibration is a combination of SV (vertical polarisation) and P (pressure) vibrations. Each mode of the families has its own dispersion curve. At high frequencies the Lamb waves degenerate to Rayleigh waves, whose velocity is independent of frequency.

The sensors produced electrical output on compression and expansion in a direction normal to their mounting surface. Thus the SH waves were excluded and only Lamb waves were detected.

The complexity associated with the wave modes generated by an emission source is formidable, as was reflected by the complex reception pattern of a sensor mounted some distance from a source. To obtain this, simulated emission pulses were injected into the vessel plate from a piezo-electric transducer resonant at 5 MHz. This transducer was excited by a step voltage so that a displacement sharp compared with the 6 μs sensor resonance period was applied to the plate. An increase in voltage to a clearly defined peak was observed, even at the largest distance, followed by an extended decay. The first energy is received at a velocity close to the P wave velocity while the peak travels with a velocity near that of shear waves in the material.

The important results were obtained that the peak energy travels with a definite velocity, 2.95×10^3 ms^{-1}, and that the amplitude of the pulse can be represented by

$$a = a_1 r^b \qquad \ldots(3.1)$$

where r is the propagation distance, b is -0.9 and a_1 is determined by the input amplitude.

It appears that the exponent of r is dependent on the vessel thickness, due to the dependence of the dispersion curves on thickness. For thick plates the exponent approaches the value -0.5, which is the maximum set by the spreading of the wavefront from the source. From thick plate studies with similar material to that of the present vessel, the intrinsic attenuation produced by the absorption and scattering of energy is about 0.2 dB metre at the experimental frequency, and can therefore be neglected.

4. RESULTS FOR VESSEL PRESSURISATION

The vessel was pressurised with water at approximately 50 psi/min (5.7 kN/m^2s). Leaks halted the test at 240 psi (1.65 MN/m^2) and 733 psi (5.05 MN/m^2). The leak st 240 psi sealed itself during a hold at this pressure but the pressure was reduced to zero to seal the high pressure leak. Several cycles to lower pressures were necessary to check and readjust the sealing before the test could proceed to the maximum pressure for the experiment, 990 psi (6.83 MN/m^2). During the final pressurisation the pressure was held at 890 psi (6.14 MN/m^2) during which the slit opening increased slowly by 0.30 mm, and again at 990 psi (6.83 MN/m^2) when the slit opening increased more rapidly to indicate the impending failure of the vessel. After 0.45 mm spontaneous slit opening the pressure was released. Figure 2 displays the increase in slit opening with pressure. Observe the nearly elastic behaviour to 220 psi (1.38 MN/m^2) followed by plastic yielding at an ever increasing rate.

During pressurisation the discrimination threshold level was conservatively set to give no output from electronic noise. We required only an instantaneous passage of the signal above this level for event

recognition. The event rate varied during the test, averaging 3 detected events per second. Figure 3 presents the results, with the actual slit position marked as a vertical line. We observe that the slit was clearly revealed by its emissions in an otherwise quiet background. When the count rate for each sensor is recalled, the absence of located noise sources is striking.

Let C be the number of outputs from the master sensor during the test period; let T be the number of times all sensors produced an output within the 800 μs time window associated with the master's output. The time window was set so that an emission event from a source anywhere on the vessel could register in the count T, given a sufficiently large event to trigger each sensor. In fact the count T principally arose from events at the slit. The count C exceeded T sixtyfold. The requirement for triplet coincidence, within the time window, was thus a powerful technique for detecting the slit in the presence of noise.

The fact that C greatly exceeds T is consistent with a substantial part of the noise background being produced by a number of low amplitude sources each emitting independently. In such a case the noise peaks are produced by the chance constructive interference of independent wave trains from these sources. The expected number T_e of triplet coincidences can then be expressed in terms of the average output number p from each sensor in unit time (assumed identical for each sensor), the time window w for coincidence and the period over which the test was conducted. Thus approximately

$$T_e = p^3 w^2 t \qquad \ldots(4.1)$$

Under the conditions of the test, namely $p = 3\ s^{-1}$, $w = 800\,\mu s$ and $t = 600$ s we find $T_e = 0.01$. Thus although C is 2000, T_e matches the very small background observed.

Signal timing uncertainty leads to the spread of emission locations each side of the slit, apparent in Figure 3. The uncertainty is associated with the method of leading edge detection employed (Connors, 1973)

together with the digital representation of the time intervals Δt_x and Δt_y (Tobias, 1973). Additionally, the 6μs resonant period of the sensors and the interference between the multiple wave modes reaching each sensor from a given event, dependent on the distance from source to sensor, affect the apparent arrival time of an emission pulse. These errors combined to broaden the apparent source width each side of the slit to 6 cm.

It is interesting to question how the emission events at the slit were distributed during the course of the pressurisation. Figure 3 presents the results for selected pressure intervals. Observe the changing emission character as the test proceeded. The slit showed little acoustic activity before 200 psi (1.38 MN/m^2). From 240 psi to 450 psi (1.65 MN/m^2 to 3.10 MN/m^2) the length of the slit was active, while from 450 to 650 psi (3.10 MN/m^2 to 4.48 MN/m^2) only the ends of the slit produced emissions. Above 700 psi (4.83 MN/m^2) acoustic activity at the slit was slight, with substantial scattered background noise in the range 890 psi to 990 psi (6.14 MN/m^2 to 6.83 MN/m^2). The slit centre gave some emissions during the spontaneous opening of the slit at the 990 psi (6.83 MN/m^2) pressure hold.

5. INTERPRETATION

The results relating emissions to pressure, location (Figure 3) and slit opening (Figure 2) are comprehensive enough to allow us to test hypotheses regarding the origin of the emissions. The adopted experimental procedure should have ruled out mechanisms extraneous to the material of the steel itself, such as flaking rust. Most laboratory-scale investigations involving C/Mn steels of the type used for the present studies show that emissions are associated with deformation (e.g. Palmer, 1972, Bentley et al., 1972) rather than with crack growth, and with the yielding process rather than with later plastic flow. The fact that the early emissions came from the centre of the slit while the later ones came from the ends suggests immediately that this is the case. Again, Figure 2 indicates* very clearly that cumulative emission number N, plotted as a function of pressure

p, is not in agreement with the curve representing the increase of slit opening with pressure - the later stages of deformation cause few emissions.

Following the hypothesis that the cumulative emission number is proportional to the yielded volume V(p), consider a simple model for the yielding such that the slit is of length L (370 mm), depth a (16.5 mm) in material of thickness W(26.9 mm). Neglect end restraints and consider the yielded zone, for pressures below that producing general yield across the slit ligament, as a cylinder of diamter S_1. From Smith (1965) we have

$$S_1 = a\left\{\left[1 - \frac{\pi^2\sigma^2}{8\sigma_y^2}\left(1 + \frac{\pi^2 a^2}{12W^2}\right)\right]^{-1} - 1\right\} \qquad \ldots (5.1)$$

Here σ_y is the yield stress and σ is the hoop stress, given for vessel diameter D by

$$\sigma = \frac{PD}{2W} \qquad \ldots (5.2)$$

The crack opening displacement (COD), δ , at the root of the slit may be expressed in terms of S_1 as

$$\delta = \frac{8\sigma_y a}{\pi E} \ln\left(1 + \frac{S_1}{a}\right) \qquad \ldots (5.3)$$

when the effects on the yielded region caused by the proximity of the inner surface of the vessel are neglected (Goodier and Field, 1963). (E is Young's modulus). This gives δ as 0.022 mm for yield across the ligament. Adding this COD to the elastic line of Figure 2 we obtain 350 psi (2.41 MN/m^2) for the pressure which produced this COD. This probably underestimates the pressure required for full yielding when we consider the ligament stress σ_ℓ given by

$$\sigma_\ell = \sigma\left(\frac{W}{W-a}\right) \qquad \ldots (5.4)$$

With expression 5.2, 420 psi (2.9 MN/m^2) is required to give σ_ℓ equal to σ_y. We shall assume 400 psi (2.76 MN/m^2) as a compromise.

---

* Because of the leaks we have estimated the emission counts in the ranges 190-250 psi and 650-730 psi

Developing the simple model for yielding further, when the entire ligament beneath the slit has yielded let a second stage of yielding occur such that the yielded volume spreads from each end of the slit out across the vessel in the form of a disc with diameter S_2. Imagine the slit to be a through thickness slit, across which is applied a stress σ modified from the hoop stress in the vessel as a result of the restraint by the ligament. Thus

$$\sigma' = \sigma - \sigma_r (W - a)/W \qquad \ldots (5.5)$$

where σ_r is the stress in the ligament. This restraining stress will rise from σ_y to the ultimate tensile stress σ_u at which ligament failure occurs.

With the assumption that the vessel plate is infinite, the diameter S_2 is given by the usual formula (Bilby, Cottrell and Swinden, 1963) as

$$S_2 = \frac{L}{2}\left(\sec \frac{\pi \sigma'}{2\sigma_y} - 1\right) \qquad \ldots (5.6)$$

Thus the total volume of yielded material is now

$$V = \frac{\pi}{4} S_1^2 L + \frac{\pi}{2} S_2^2 W \qquad \ldots (5.7)$$

Figure 4 displays V(p) from this expression, with two assumptions for the restraining stress:

1) $\sigma_r = \frac{1}{2}(\sigma_y + \sigma_u)$

and 2) $\sigma_r = \sigma_u$

Figure 4 also presents the cumulative emission count N(p), from which it is seen that N(p) is in broad agreement with V(p). The fall in emission rate after the steep rise at 350 psi (2.4 MN/m^2) is particularly striking.

The model for V(p) is of course a gross simplification. More realistically we would expect a smooth transition between the first and second stages of yielding so that emission activity would move from centre to ends of the slit, and this is demonstrated in Figure 3. It appears that the restraint of the ligament is closer to assumption (2) above, so

that the yield in the vessel plate at each end of the slit is small. The results strongly suggest that the emission activity detected arose primarily from first yielding of the material.

It can be seen from Figure 4 that the number N of emissions above 5.1 μv threshold amplitude was approximately related to the volume V by

$$N = 2V \qquad \ldots(5.8)$$

when V is measured in cm^3.

6. APPLICATION TO DEFECT LOCATION

In order to avoid excessive count rates from noise it is necessary to set threshold discriminators so as to reject signals below a given amplitude. Thus in order to assess the application of acoustic emission to NDT examination of vessels it is important to know the amplitude of emissions from defects.

If we represent the number $n(a)$ of events with amplitude in the interval a to a + da by

$$n(a) = Aa^x \qquad \ldots(6.1)$$

then the number of events $N(a_t)$ above a threshold level a_t is

$$N(a_t) = \int_{a_t}^{\infty} n(a)\, da$$

$$= -\frac{A}{x+1}\, a_t^{x+1} \qquad \ldots (6.2)$$

so that $\log N(a_t) = -\log\left(\frac{A}{x+1}\right) + (x+1)\log a_t$

Figures 2 and 3 were derived with noise backgrounds of up to 10 cps at each sensor, and sensor M was set at 5.1 μv to achieve this. To determine how the emission count depended on discriminator setting we replayed the magnetic tape recorded in the experiment, varying the setting of discriminator M while maintaining the discriminators for X and Y to give 10 cps noise.

Analysing the results in the above manner (equation 6.2) gave:

$$N(a_t) = 173\ a_t^{-1.33}$$

and hence

$$n(a) = 230\ a^{-2.33} \qquad \ldots(6.3)$$

where a_t and a are in microvolts.

It is interesting to apply this result and derive the effect of sensor spacing. For detection of a source by a sensor at distance r using a threshold a_t, an emission signal from the source must have amplitude exceeding a_o at r_o, where from equation 3.1

$$a_o = a_t \left(\frac{r_o}{r}\right)^b \qquad \ldots(6.4)$$

With the assumption that all events at the slit arose from the slit centre, and recalling that the sensor spacing was 1.02 m, it is then easy to show that for sensor spacing d, the detected number of events N would be given as

$$N = N_o\ a_t^{x+1}\ d^{-b(x+1)}\ V \qquad \ldots(6.5)$$

Under the conditions of the experiment, using expression 5.8, we have

$$N = 18\ a_t^{-1.33}\ d^{-1.2}\ V \qquad \ldots(6.6)$$

where a_t is in microvolts, d is in metres and V is in cm^3.

This useful result can be applied to structures for which NDT by acoustic monitoring during proof test is required. We would wish N to significantly exceed the noise background in the area of surveillance, which can be derived from expression 4.1 when noise is uncorrelated at each sensor. With given sensor spacing, amplitude threshold level and background noise count we can then determine the minimum yielded volume which would be detected during a test. In turn this would be related to the minimum detectable defect size.

Conversely, if the minimum defect size significant to structural integrity is known, together with the background noise, then the maximum sensor spacing for detection is determined.

It should be recognised that expression 6.6 relates to steel with the particular composition and heat treatment of the test vessel. The exact behaviour of any other steel will depend on its composition and microstructure.

7. CONCLUSIONS

1. The equipment is successful under the conditions adopted in locating areas of yielding. Considerable background noise can be accommodated.
2. The emissions observed were caused by yielding of material near the slit. This does not exclude the possibility of emissions from crack growth itself, in more brittle materials.
3. Such emission from yielding material will be observed even when crack growth is silent, since fresh yielding is always associated with crack growth. In any event, the occurrence of yielding at stresses lower than the initial proof test and after a period of service would indicate a serious condition.

REFERENCES

Auld, B.A., 1973, "Acoustic Fields and Waves in Solids" Wiley, New York

Bentley, P.G., Burnup, T.E., Burton, E.J., Cowan, A. and Kirby, N., 1972 Conference "Periodic Inspection of Pressure Vessels" London, Inst. Mech. Eng., 9-11 May, 1972. p.54.

Bentley, P.G., Burton, E.J., Cowan, A., Dawson, D.G. and Ingham, T., 1973 Second International Conference on Pressure Vessel Technology, San Antonio, 1973, p.643

Bilby, B.A., Cottrell, A.H. and Swinden, K.H., 1963, Proc. Roy. Soc., A272 304

Connors, D.C., 1973, C.E.G.B. Report RD/B/N2626

Goodier, J.N. and Field, F.A., 1963, "Fracture of Solids", p.103, Interscience, New York.

Nakamura, W., Veach, C.L. and. McCauley, B.O., 1971, "Acoustic Emission" ASTM Publication 505

Palmer, I.G., 1972, C.E.G.B. Report RD/L/N133/72

Parry D.L., and Robinson, D.L., 1970, Jersey Nuclear Report IN-1398

Smith, E., 1965, Proc. Roy. Soc. A285, 46

Tobias, A., 1973, C.E.G.B. Report RD/B/N2854

Vetrano, J.B., Jolly, W.D. and Hutton, P.H. 1972, Conference "Periodic Inspection of Pressure Vessels", London, Inst. Mech. Eng. 9-11 May 1972 p.221.

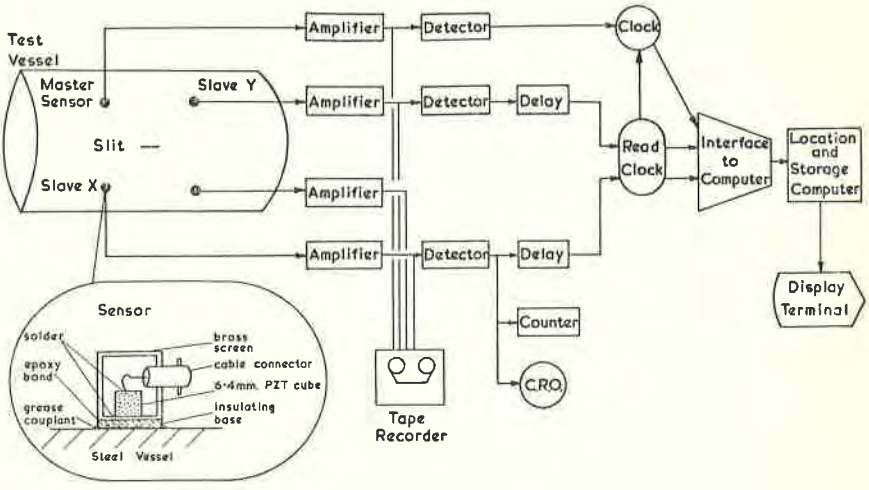

Figure 1. Acoustic emission detecting system.

Table 1

Specification of Steel

Silicon killed C/Mn steel plate normalised at 950°C

Vessel stress relieved at 600°C for 2 hours

Composition	C	Si	S	P	Mn	Ni	Cr	Mo	Cu	Sn
Wt.%	.185	.21	.023	.024	.80	.13	.168	.015	.13	.011

Yield stress σ_y = 35.8 x 10^3 psi (247 MN/m^2)

Ultimate tensile stress σ_u = 62.9 x 10^3 psi (434 MN/m^2)

Young's modulus E = 2.98 x 10^7 psi (205 GN/m^2)

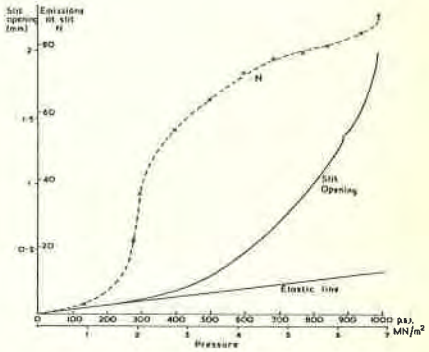

Figure 2. Slit opening and cumulative emission count as a function of pressure.

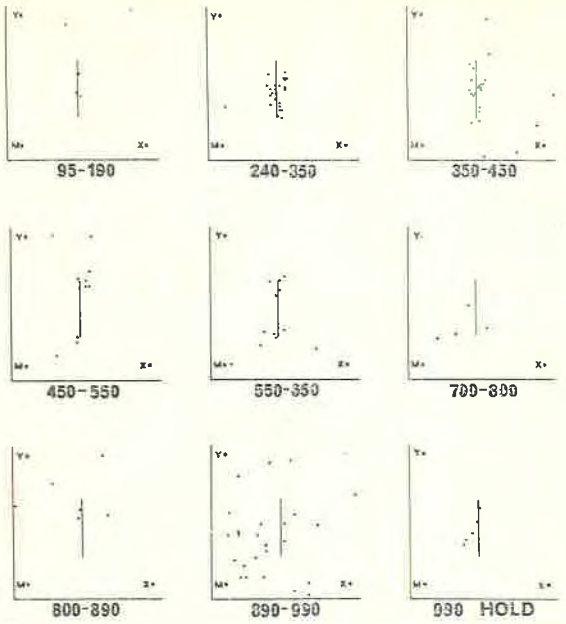

FIG 3. EMISSION EVENTS AS A FUNCTION OF PRESSURE.

PRESSURES ARE GIVEN IN p.s.i.

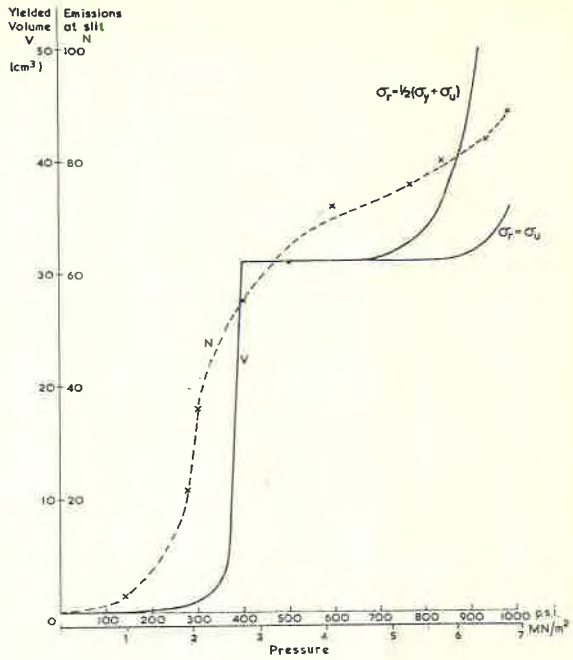

Figure 4. Yielded volume and cumulative emission count as a function of pressure.